ACS APPLIED MATERIALS & INTERFACES

Research Article

www.acsami.org

Deep-Red Emissive Crescent-Shaped Fluorescent Dyes: Substituent Effect on Live Cell Imaging

Weimin Liu,[†] Bingjiang Zhou,[†] Guangle Niu, Jiechao Ge, Jiasheng Wu, Hongyan Zhang, Haitao Xu, and Pengfei Wang*

Key Laboratory of Photochemical Conversion and Optoelectronic Materials and CityU-CAS Joint Laboratory of Functional Materials and Devices, Technical Institute of Physics and Chemistry, Chinese Academy of Sciences, Beijing 100190, People's Republic of China

Supporting Information

ABSTRACT: A series of crescent-shaped fluorescent dyes (**CP1**−**CP6**) were synthesized by hybridizing coumarin and pyronin moieties with different amino substituents at both ends. The molecular structures and photophysical properties of these fluorescent dyes were investigated through X-ray diffraction, absorption spectroscopy, and fluorescence spectroscopy. Results show that the fluorescent dyes exhibited crescent-shaped structures, deep-red emissions (approximately 650 nm), and significant Stokes shifts. In live-cell-imaging experiments, **CP1** stains mitochondria, whereas **CP3** and **CP6** stain the lysosomes in a cytoplasm and the RNA in nucleoli. The relationships between different amino substituent groups and the imaging properties of **CP** dyes were discussed as well. Additionally, findings from the cytotoxicity and photostability experiments on living cells indicated the favorable biocompatibility and high photostability of the **CP** dyes.

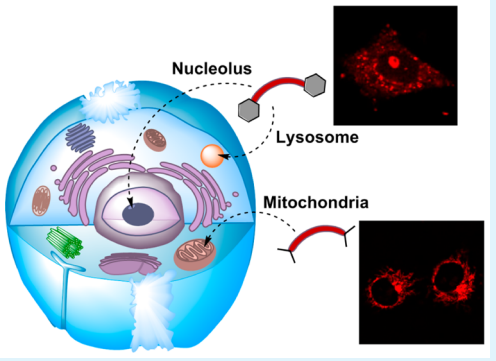

KEYWORDS: *fluorescent dyes, bioimaging, nucleolus, lysosome, mitochondria*

INTRODUCTION

Cells contain many small elements known as organelles, which perform specific functions related to the life and health of cells. For example, the mitochondrion is an important area from which to produce the energy currency of the cell through respiration and to regulate cellular metabolism.[1−3] Lysosomes act as the waste disposal system of the cell by digesting virtually all types of macromolecules taken in during the processes of phagocytosis, endocytosis, and autophagy.[4,5] The nucleolus performs a key function in ribosome biogenesis. The number, size, and activity of nucleoli increase in exponentially growing cells.[6,7] Therefore, the visualization of organelles is critical to understanding their intracellular function. In line with this need, several imaging techniques have been developed to visualize and study specific organelles, such as the electron microscopy study of cell structures,[8] silver staining for the nucleolar organizer region,[9,10] and fluorescent imaging using different fluorescent probes.[11−14] Among these imaging techniques, fluorescence imaging technology that uses organic molecules is a powerful tool for cell imaging.[15−17] Especially, small-molecule fluorescent probes can permeate the cell membrane and can be used on organelle visualization in living cells.[18−20] As a result, organelle operation can be established. The output of this method is better than the snapshots captured by imaging studies on fixed cells.[21−24]

The design and synthesis of fluorescent dyes is essential to fluorescent molecular imaging, and much effort has been exerted to exploit new dyes, especially long-wavelength dyes (>600 nm).[25−27] Fluorescence imaging excited with deep-red light induces minimal photodamage in living cells.[28−30] Moreover, interference from the background autofluorescence of biomolecules in the cells is negligible. Nonetheless, fluorescent dyes with brand-new structures and excellent properties are rare. The rigid hybridization of two classical fluorescent dyes is a novel, efficient strategy for the design of new fluorescent dyes.[31−37] Such dyes display the following advantages: (1) favorable photostability and high fluorescence quantum yields as a result of the rigid structure; (2) extraordinary properties aside from retaining the individual advantages of each classical dye. For instance, we recently constructed a novel fluorescent dye (**CP4**; Scheme 1) by hybridizing coumarin and pyroine moieties.[38] This dye not only exhibited excellent photophysical properties, such as deep-red emission wavelength, excellent fluorescence quantum yields, favorable photostability, and significant Stokes shifts, but also stained the RNA in the nucleoli of living cells selectively. Although **CP4** can permeate nucleoli easily, the factors that influence nuclear membrane permeability are unknown.

In the current study, we design and synthesize a series of crescent-shaped fluorescent dyes (**CP1**, **CP3**, and **CP6**; Scheme 1) with different amino substituents at both ends. For comparison, we also synthesize **CP2** and **CP5** to determine nuclear membrane permeability. The structure of **CP1** has been published by Haucke et al.,[39] but its synthetic method and

Received: February 14, 2015
Accepted: March 18, 2015
Published: March 18, 2015

DOI: 10.1021/acsami.5b01429
ACS Appl. Mater. Interfaces 2015, 7, 7421−7427

Scheme 1. Structure of CP Dyes

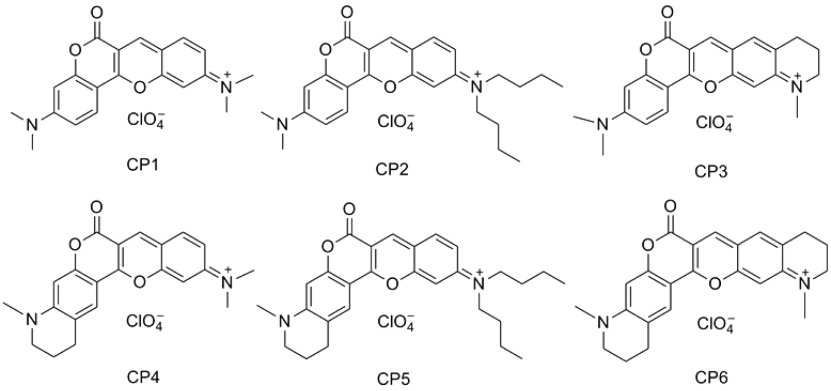

application in bioimaging have not been reported. The properties of these **CP** dyes are investigated through X-ray diffraction, absorption spectroscopy, fluorescence spectroscopy, and confocal laser scanning microscopy. As in **CP4**, clear nucleolus and lysosome staining was observed in living cells for **CP3** and **CP6**. These two dyes contain 1-methyl-1,2,3,4-tetrahydroquinoline parts at one or both ends. Surprisingly, **CP1** with *N*,*N*-dimethylaniline at both ends can localize stably in mitochondria. Thus, the different organelle stain of **CP** dyes can be obtained by regulating different amino substituents.

RESULTS AND DISCUSSION

Synthesis and Characterization. In our previous work,[38] a crescent-shaped dye (**CP4**) with positive charges exhibited good cell membrane permeability and could stain the nucleoli and lysosomes of living cells. To study the steric effect of substituents and the size effect of crescent shapes, we synthesized a series of crescent-shaped **CP** dyes containing different amino substituents at both ends. The detailed synthetic routes and methods of **CP** dyes are shown in Scheme 2. Compounds **5** and **6** were acquired through interesterification and the Friedel–Crafts reaction of aminophenol (compound **1** or **2**) with compound **4**. Compounds **7** and **8** were synthesized through a Vilsmeier–Haack reaction.

Scheme 2. Synthesis of CP Dyes[a]

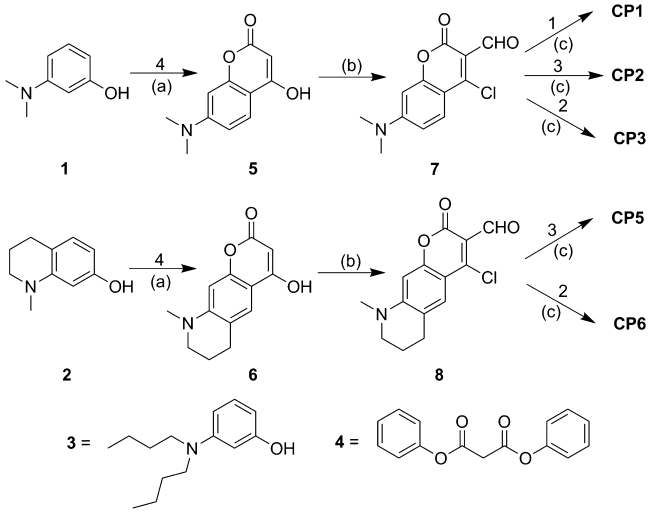

[a]Conditions: (a) toluene, reflux, 6 h; (b) phosphoroxychloride/dimethylformamide, 50 °C, 30 min; (c) acetic acid, 85 °C, 2 h.

Eventually, **CP1**–**CP3**, **CP5**, and **CP6** were obtained through the condensation reaction of compounds **7** and **8** with relative aminophenol. The overall chemical structures of **CP** dyes were confirmed via ^{1}H and ^{13}C NMR and electrospray ionization high-resolution mass spectroscopy (ESI-HRMS; Figure S1 in the Supporting Information, SI).

Single crystals of **CP6** that were suitable for X-ray crystallographic analysis were obtained by the slow evaporation of CH_3OH and CH_3COOH solutions of **CP6** at ambient temperature. The details of the X-ray experimental conditions and cell and refinement data of **CP6** are summarized in Table S1 in the SI. The molecular structures of **CP6** were elucidated through X-ray crystallography, which revealed a coumarin- and pyronin-fused skeleton that formed a triclinic unit cell and a $P\bar{1}$ space group (Figure 1). The **CP6** skeleton without C3 and C22

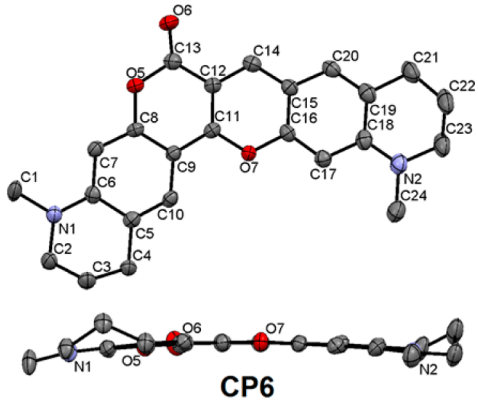

Figure 1. ORTEP views of the molecular structures of **CP6** with thermal ellipsoids shown at 50%. All hydrogen and partial carbon atoms have been omitted for clarity.

of the six-membered ring at both ends is highly planar, with a torsion angle C5–C10–C18–C19 of θ = 171.040°. This angle indicates the strong π-electron delocalization within the two main planes. X-ray crystallographic data showed that the C–N bond length r values of **CP6** are 1.458 and 1.477 Å, thus implying delocalization of the positive charge. The molecule curve radian, which is the angle of C4–C11–N2, is 111.500°.

Spectral Properties. We investigated the absorption and fluorescence spectra of **CP** dyes in CH_2Cl_2 or tris-(hydroxymethyl)aminomethane–ethylenediaminetetraacetic acid (TE) buffer solution (pH = 7.4; Figure S2 in the SI). The corresponding photophysical data are summarized in Table 1. The absorption of **CP** dyes is maximized in the region ranging

DOI: 10.1021/acsami.5b01429
ACS Appl. Mater. Interfaces 2015, 7, 7421–7427

Table 1. Photophysical Data of CP Dyes

dye	solvent	λ_{max} (nm)	λ_{em} (nm)	Stokes shift (nm)	ε (M^{-1} cm^{-1})	Φ
CP1	CH_2Cl_2	606	632	26	82800	0.537
	TE buffer	589	639	50	47000	0.024
CP2	CH_2Cl_2	610	634	24	94400	0.377
	TE buffer	594	640	56	41000	0.044
CP3	CH_2Cl_2	604	630	26	152800	0.555
	TE buffer	584	638	54	67000	0.041
CP4[38]	CH_2Cl_2	618	648	30	80800	0.215
	TE buffer	598	658	60	39000	0.01
CP5	CH_2Cl_2	623	649	26	63800	0.251
	TE buffer	604	657	53	42000	0.017
CP6	CH_2Cl_2	616	648	32	86400	0.338
	TE buffer	595	655	60	51000	0.015

from 584 to 600 nm. Emission is maximized at 638−658 nm in a TE buffer solution. Compared with **CP1**−**CP3**, **CP4**−**CP6** red shift during the absorption and fluorescence peaks because of the increasing donor property of the amino group in the coumarin moiety. Therefore, the fluorescence quantum yields for **CP4**−**CP6** are low given that the energy gap decreases.[40,41] The Stokes shift (50−60 nm) of **CP** dyes is more significant than that of xanthene dyes in aqueous solution. This shift can reduce self-absorption, as well as determine the high-resolution and low-detection limits. The high molar extinction coefficients exceed 10^4 M^{-1} cm^{-1} in all **CP** dyes. Moreover, the fluorescence quantum yields of **CP** dyes range from 0.215 to 0.555 in CH_2Cl_2. These yields are significant for deep-red fluorescent dyes. However, the fluorescence quantum yields of **CP** dyes range from only 0.01 to 0.044 in a TE buffer solution. Thus, the striking difference in the fluorescence quantum yields in different environments can provide a strong contrast and almost no background for bioimaging.

Fluorescent Imaging Properties. Laser confocal imaging experiments were conducted to study the cellular distribution of **CP** dyes in HeLa cells (Figure 2a). **CP1**, **CP3**, and **CP6** easily permeated the living cells upon loading in a culture medium at optimum concentration, with the exception of **CP2** and **CP5**. The cell morphology or viability did not change significantly during the imaging process (Figure 2b). **CP1** was mainly localized at the cytoplasm, and the nucleus was not obviously stained at a concentration of 5 μM. However, a very slight stain in the nucleus can be observed at an increased concentration (10 μM), along with the high cytotoxicity of **CP1** (Figure S3). On the contrary, the nucleolus in the nucleus was clearly stained by **CP3** and **CP6**, as indicated by the bright spots in the cytoplasm (Figure 2a). On the basis of the results above, the closed loop at one or both ends of **CP** dyes may be an important factor in favorable nuclear membrane permeability. Moreover, the hydrophilicity/hydrophobicity of dyes also affects cell/nuclear membrane permeability significantly. The large lipophilic groups of **CP2** and **CP5** hinder the dyes from entering the cell, although **CP5** exhibits a closed-loop structure at one end. As presented in Figure 2, the nucleoli unstaining of **CP2** and **CP5** even at 20 μM also highlighted the importance of appropriate hydrophobicity to nuclear membrane permeability.

Interestingly, the localization of **CP1** with *N*,*N*-dimethylaniline at both ends in a cytoplasm is different from that of other **CP** dyes. Colocalization experiments demonstrated that fluorescence throughout in the cytoplasm is predominantly associated with mitochondria for **CP1** (Figure 3a). However, **CP3** and **CP6** can specifically localize in lysosomes (Figure 3b), as with **CP4**.[38] Positively charged moieties accumulate in either mitochondria or lysosomes.[18,19] The varying stains of **CP** dyes on organelles can extend the applicability of such dyes in cell imaging. In addition, the dyes may exhibit different cell-staining behaviors in varied cell lines. Thus, we investigated **CP1**, **CP3**, and **CP6** staining in other common cell lines (cancer cell A549 and normal cell L929). Figure 4 shows that staining is similar in

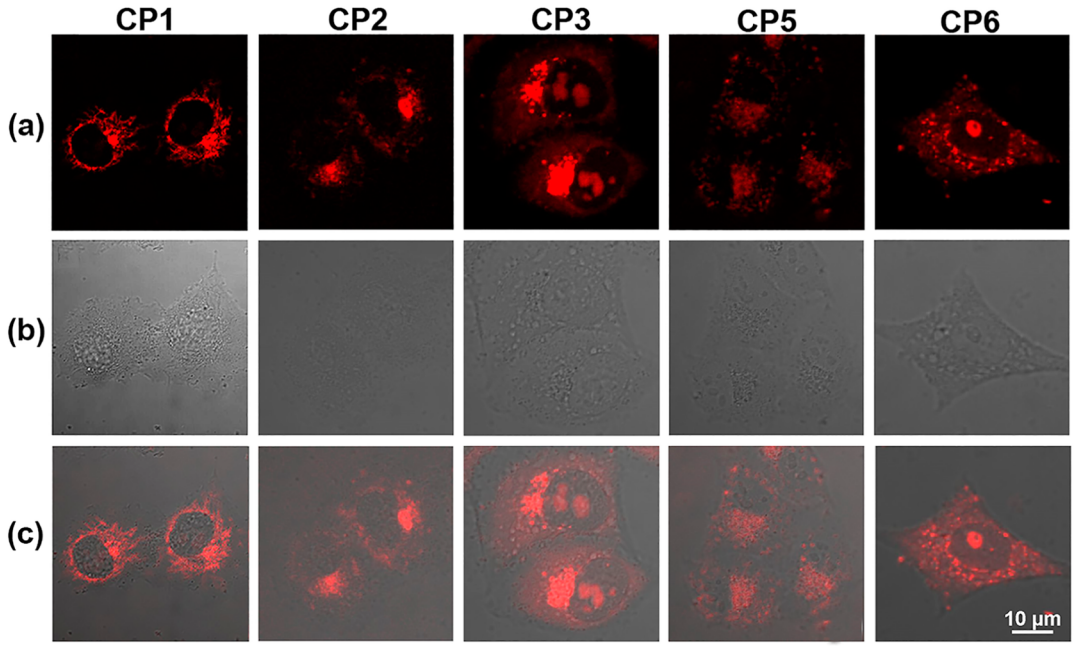

Figure 2. Live cell imaging of HeLa cells with **CP** dyes: (a) fluorescence imaging of **CP** dyes; (b) bright-field image; (c) overlay of parts a and b. [**CP1**] = 5 μM, [**CP2**] = 20 μM, [**CP3**] = 7 μM, [**CP5**] = 20 μM, and [**CP6**] = 7 μM.

DOI: 10.1021/acsami.5b01429
ACS Appl. Mater. Interfaces 2015, 7, 7421−7427

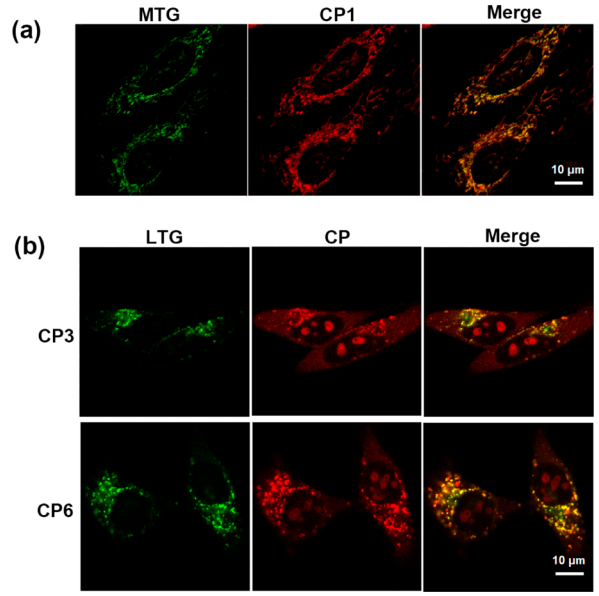

Figure 3. Colocalization of **CP1** with MitoTracker Green (MTG) (a) and **CP3** and **CP6** with LysoTracker Green (LTG) (b) in HeLa cells. [**CP1**] = 5 μM, [**CP3**] = 7 μM, [**CP6**] = 7 μM, [MTG] = 50 nM, and [LTG] = 50 nM.

the two cell lines, thus indicating that **CP1**, **CP3**, and **CP6** can be used to image cancerous and normal cells.

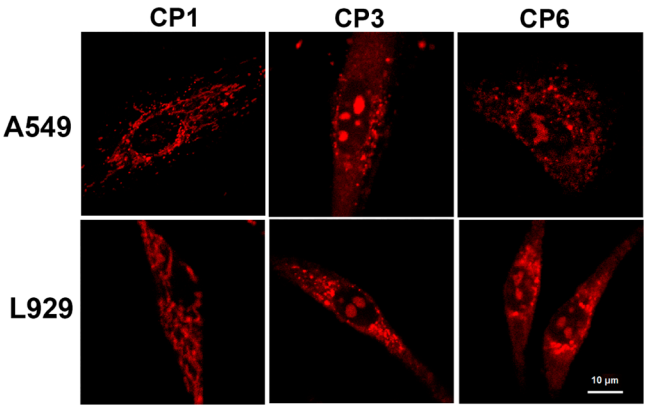

Figure 4. Live cell imaging of A549 and L929 cells with **CP1**, **CP3**, and **CP6**. [**CP1**] = 5 μM, [**CP3**] = 7 μM, and [**CP6**] = 7 μM.

To confirm that **CP3** and **CP6** stain the RNA in nucleoli selectively as with **CP4**, deoxyribonuclease (DNase) and ribonuclease (RNase) digest experiments were performed using fixed-permeabilized HeLa cells. SYTO RNASelect was tested as a control. As depicted in Figure 5, fluorescence in the nucleoli was not significantly lost for **CP3**, **CP6**, and RNASelect upon treatment with DNase. By contrast, the fluorescence signals of **CP3**, **CP6**, and RNASelect were completely lost in the nucleoli after RNase digestion. These results indicate that **CP3** and **CP6** mainly stain the RNA in nucleoli.[38,43]

Cytotoxicity and Photostability. Cytotoxicity and photostability are important factors in evaluating the applicability of new fluorescent probes for live cell imaging. Thus, the cytotoxicity of **CP1**, **CP3**, and **CP6** to HeLa cell lines was studied by using a standard 3-(4,5-dimethylthiazol-2-yl)-2,5-diphenyl-2*H*-tetrazolium (MTT) assay after 24 h of incubation

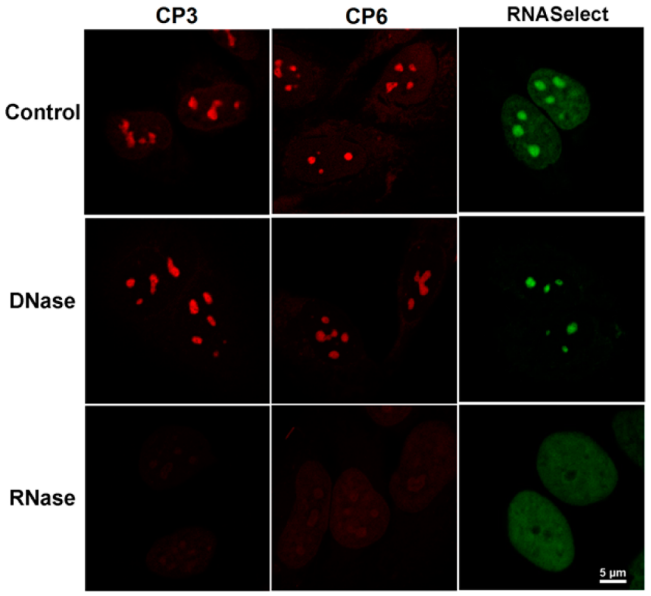

Figure 5. DNase and RNase digest experiments in fixed HeLa cells. [**CP3**] = 1 μM, [**CP6**] = 1 μM, and [SYTO RNASelect] = 0.5 μM.

(Figure 6a). Three dyes exhibit good cell tolerability at imaging concentration after 24 h of incubation. Among all of the **CP**

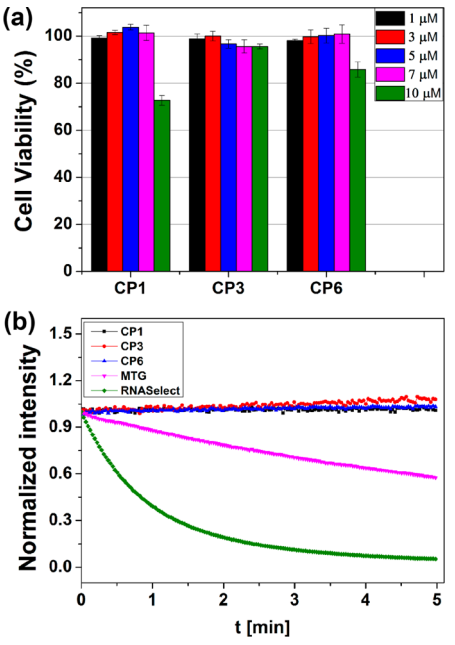

Figure 6. (a) Cytotoxicity of **CP** dyes in Hela cells. (b) Photostability of **CP** dyes, MTG, and SYTO RNAselect in cell imaging. [**CP1**] = 5 μM, [**CP3**] = 7 μM, [**CP6**] = 7 μM, [MTG] = 100 nM, and [SYTO RNASelect] = 0.5 μM.

dyes, **CP1** displayed slight cytotoxicity at high concentrations. We compared the imaging properties of **CP** dyes, MTG, and SYTO RNASelect dye through photostability experiments. The three **CP** dyes exhibited better photostability than MTG and SYTO RNASelect did (Figure 6b). Furthermore, the fluorescent intensity did not decrease under imaging as in **CP4**. Good photostability is necessary for the use of a dye in cell imaging, especially for long-term illumination. The results reveal that the three dyes are promising and can be used for the

DOI: 10.1021/acsami.5b01429
ACS Appl. Mater. Interfaces 2015, 7, 7421−7427

long-term imaging of mitochondria, lysosomes, or RNA in nucleoli.

CONCLUSIONS

A series of crescent-shaped, deep-red emission **CP** dyes that contain coumarin- and pyronin-fused conjugated skeletons were designed and synthesized based on our previous work. The hybridization of coumarin and pyronin Y moieties induces significant stock shifts and long-wavelength emissions. The results of live cell fluorescence imaging experiments indicate that different amino substituents significantly influence the imaging properties of **CP** dyes, including cell membrane permeability, nuclear membrane permeability, and the organelle location. **CP1**, **CP3**, and **CP6** can stain various organelles in living cells. Moreover, they possess low cell cytotoxicity and high photostability, which makes **CP** dyes good options for monitoring the dynamic changes in mitochondria, lysosomes, or nucleoli in living cells. This design strategy may be extended to the development of other fluorescent dyes for live cell imaging.

EXPERIMENTAL SECTION

Materials and Measurements. All commercial chemicals were used without further purification. The stock solutions of **CP** dyes were prepared in dimethyl sulfoxide (DMSO; 1.0×10^{-2} M). Water was purified by a Millipore filtration system. Fluorescence quantum yields were measured with cresyl violet in methanol as the reference (Φ_f = 0.54).[38,44] All measurements were taken at room temperature. All UV−vis and fluorescence spectra in this work were recorded by Hitachi U3010 and F4500 fluorescence spectrometers. ^{1}H (400 MHz) and ^{13}C (100 MHz) NMR spectra were collected on a Bruker Advance 400 spectrometer with tetramethylsilane as an internal standard. ESI-HRMS spectra were obtained on a Bruker Apex IV Fourier transform mass spectrometer. Images were acquired with a Nikon C1si laser scanning confocal microscope equipped with a live cell incubation chamber that maintained a humidified atmosphere of 37 °C and 5% CO_2.

Synthesis. *Synthesis of 7-(Dimethylamino)-4-hydroxycoumarin (**5**).* 3-(Dimethylamino)phenol (**3**; 1.37 g, 10.0 mmol) and diphenyl malonate (**4**; 2.56 g, 10.0 mmol) were added into anhydrous toluene (15 mL). The mixture was refluxed for 6 h, and compound **5** was obtained by filtration as hoar solid (1.30 g, 63.4%). ^{1}H NMR (400 MHz, DMSO-d^6): δ 11.93 (s, 1H), 7.55 (d, J = 8.9 Hz, 1H), 6.68 (dd, J = 9.0 and 2.4 Hz, 1H), 6.47 (d, J = 2.4 Hz, 1H), 5.26 (s, 1H), 2.99 (s, 6H). ^{13}C NMR (100 MHz, DMSO-d^6): δ 166.55, 162.76, 155.70, 153.27, 123.78, 108.52, 104.10, 97.12, 86.42. ESI-HRMS. Calcd for $[C_{11}H_{11}NO_3 + Na]^+$: m/z 228.06276. Found: m/z 228.06276.

*Synthesis of 4-Chloro-7-(dimethylamino)coumarin-3-carbaldehyde (**7**).* To 3 mL of dry dimethylformamide was slowly added 2 mL of phosphoroxychloride, and the resulting mixture was heated for 30 min at 50 °C. Compound **5** (1.03 g, 5.0 mmol) was dissolved in 10 mL of dimethylformamide, and the resulting solution was added dropwise into the mixture. The mixture was stirred for 6 h at 60 °C and poured into 20 mL of ice water to obtain an orange solid (1.10 g, 87.6%). ^{1}H NMR (400 MHz, $CDCl_3$): δ 10.30 (s, 1H), 7.86 (d, J = 9.3 Hz, 1H), 6.71 (dd, J = 9.3 and 2.5 Hz, 1H), 6.44 (d, J = 2.5 Hz, 1H), 3.16 (s, 6H). ^{13}C NMR (100 MHz, $CDCl_3$): δ 186.92, 159.76, 156.01, 155.44, 154.09, 128.95, 111.36, 110.66, 107.85, 96.89, 40.33. ESI-HRMS. Calcd for $[C_{12}H_{10}ClNO_3 + Na]^+$: m/z 274.02469. Found: m/z 274.02340.

*Synthesis of Compound **8**.* Compound **8** was synthesized from compound **2** according to our previous report.[38] ^{1}H NMR (400 MHz, $CDCl_3$): δ 10.28 (s, 1H), 7.53 (s, 1H), 6.32 (s, 1H), 3.48 (t, J = 6.0 Hz, 2H), 3.07 (s, 3H), 2.80 (t, J = 6.0 Hz, 2H), 2.00 (m, 2H). ^{13}C NMR (100 MHz, $CDCl_3$): δ 186.06, 159.42, 154.58, 153.32, 152.07, 125.43, 121.48, 109.84, 107.07, 95.11, 50.74, 38.79, 26.48, 20.32. ESI-HRMS. Calcd for $[C_{14}H_{12}ClNO_3 + H]^+$: m/z 278.05785. Found: m/z 278.05804.

*Synthesis of **CP** Dyes.* Compound **7** (1 mmol) or **8** (1 mmol) and compound **1**, **2**, or **3** (1 mmol) were heated for 2 h at 85 °C in 3 mL of acetic acid. After cooling, to the mixture was added 2.0 mL of perchloric acid (70%). A blue-violet power solid was precipitated by the dropwise addition of water. Filtration and drying in vacuo, a blue-violet powder was obtained. The crude product was purified by column chromatography using 50:1 (v/v) CH_2Cl_2/CH_3OH as the eluent and recrystallized from absolute methanol to afford **CP** dyes as deep-green powders.

CP1. Yield: 17.3%. ^{1}H NMR (400 MHz, DMSO-d^6): δ 8.93 (s, 1H), 8.01 (t, J = 7.0 Hz, 2H), 7.38 (d, J = 9.3 Hz, 1H), 7.27 (s, 1H), 7.04 (d, J = 9.3 Hz, 1H), 6.75 (s, 1H), 3.37 (s, 6H), 3.22 (s, 6H). ^{13}C NMR (100 MHz, DMSO-d^6): δ 162.34, 158.67, 158.21, 157.19, 156.99, 156.80, 145.20, 133.98, 125.99, 116.87, 116.45, 111.82, 105.49, 100.16, 97.76, 97.55, 41.15, 40.35. ESI-HRMS. calcd for $[C_{20}H_{19}N_2O_3]^+$: m/z 335.13902. Found: m/z 335.13862.

CP2. Yield: 14.9%. ^{1}H NMR (400 MHz, CD_3OD): δ 8.77 (s, 1H), 8.13 (d, J = 9.3 Hz, 1H), 7.89 (d, J = 9.4 Hz, 1H), 7.31 (dd, J = 9.4 and 2.1 Hz, 1H), 7.18 (s, 1H), 7.00 (d, J = 9.3 Hz, 1H), 6.69 (s, 1H), 3.72 (t, 4H), 3.26 (s, 6H), 1.75 (m, 4H), 1.48 (m, J = 6.7 Hz, 4H), 1.03 (t, J = 7.3 Hz, 6H). ^{13}C NMR (100 MHz, DMSO-d^6): δ 162.34, 158.20, 157.49, 157.43, 156.89, 156.68, 144.89, 134.17, 126.13, 116.83, 116.49, 111.54, 105.41, 100.11, 97.66, 97.32, 51.30, 40.23, 28.92, 19.32, 13.66. ESI-HRMS. calcd for $[C_{26}H_{31}N_2O_3]^+$: m/z 419.23292. Found: m/z 419.23238.

CP3. Yield: 16.8%. ^{1}H NMR (400 MHz, DMSO-d^6): δ 8.76 (s, 1H), 8.01 (d, J = 9.2 Hz, 1H), 7.72 (s, 1H), 7.23 (s, 1H), 7.03 (d, J = 9.3 Hz, 1H), 6.75 (s, 1H), 3.70 (t, 2H), 3.34 (s, 3H), 3.21 (s, 6H), 2.85 (t, 2H), 1.96 (m, 2H). ^{13}C NMR (100 MHz, DMSO-d^6): δ 161.43, 158.19, 156.76, 156.49, 156.39, 156.26, 142.73, 130.04, 127.80, 125.46, 116.90, 111.42, 104.74, 99.98, 96.42, 51.85, 40.42, 40.13, 26.29, 19.78. ESI-HRMS. Calcd for $[C_{22}H_{21}N_2O_3]^+$: m/z 361.15467. Found: m/z 361.15489.

CP5. Yield: 16.2%. ^{1}H NMR (400 MHz, CD_3OD): δ 8.73 (s, 1H), 7.86 (d, J = 9.4 Hz, 1H), 7.81 (s, 1H), 7.26 (d, J = 9.4 Hz, 1H), 7.15 (s, 1H), 6.58 (s, 1H), 3.70 (t, J = 7.8 Hz, 4H), 3.59 (t, J = 5.7 Hz, 2H), 3.18 (s, 3H), 2.88 (t, J = 6.1 Hz, 2H), 2.01 (m, 2H), 1.70 (m, 4H), 1.46 (m, 4H), 1.03 (t, J = 7.3 Hz, 6H). ^{13}C NMR (100 MHz, DMSO-d^6): δ 161.57, 158.31, 157.51, 157.31, 156.63, 154.19, 144.94, 134.19, 123.03, 122.61, 116.46, 115.98, 105.49, 99.68, 97.30, 96.56, 51.27, 51.02, 28.96, 26.43, 20.54, 19.45, 13.79. ESI-HRMS. Calcd for $[C_{28}H_{33}N_2O_3]^+$: m/z 445.24857. Found: m/z 445.24777.

CP6. Yield: 20.1%. ^{1}H NMR (400 MHz, DMSO-d^6): δ 8.74 (s, 1H), 7.69 (s, 2H), 7.18 (s, 1H), 6.64 (s, 1H), 3.68 (s, 2H), 3.53 (s, 2H), 3.31 (d, J = 4.6 Hz, 3H), 3.13 (s, 3H), 2.81 (s, 4H), 1.94 (s, 4H). ^{13}C NMR (100 MHz, DMSO-d^6): δ 161.11, 158.24, 156.81, 156.28, 156.22, 153.76, 143.00, 130.08, 127.43, 122.58, 122.39, 116.37, 104.80, 99.55, 96.35, 51.80, 50.85, 40.31, 26.40, 26.33, 20.51, 19.89. ESI-HRMS. Calcd for $[C_{24}H_{23}N_2O_3]^+$: m/z 387.17032. Found: m/z 387.16994.

Cell Culture and Staining. HeLa (uterine cervix cancer cell line), A549 (nonsmall cell lung cancer cell line), and L929 (fibroblasts cell line) cells were provided by the Cell Center at the Peking Union Medical College. Specifically, the L929, A549, and HeLa cells were grown in RPM1640, McCoy's 5A, and Dulbecco's Modified Eagle Medium (DMEM), respectively. They were supplemented with 10% fetal bovine serum and 1% penicillin/streptomycin. They were then incubated under 5% CO_2 at 37 °C. The cells were seeded on a confocal dish for imaging 12−24 h prior to the experiment. The **CP** dyes were dissolved in DMSO to a final concentration. Upon the addition of the appropriate amount of a dye stock solution directly to the culture medium, the cells were then incubated for 20 min at 37 °C in 5% CO_2 and then imaged in a dye medium under this atmosphere without washing. For colocalization experiments, **CP** dyes incubated with HeLa cells were seeded on coverslips in DMEM for 20 min. The medium was replaced with a fresh medium in the presence of MTG (a commercially available mitochondria-specific staining probe) or LTG (a commercially available lysosome-specific staining probe) for another

DOI: 10.1021/acsami.5b01429
ACS Appl. Mater. Interfaces 2015, 7, 7421−7427

20 min. The coverslips were twice washed with phosphate-buffered saline (PBS) and imaged.

DNase and RNase Treatment. The HeLa cells were fixed in prechilled methanol at −20 °C for 1 min. The cell membrane was permeabilized with 1% Triton X-100 in PBS for 1 min at room temperature. Upon rinsing twice with PBS, 0.5 μL each of a 10 mM dye stock solution and a 1 mL PBS solution were added. The cells were then incubated in this dye PBS solution for 20 min at room temperature before they were rinsed clean by PBS twice. A total of 1 mL of clean PBS (as the control experiment), 20 μg/mL DNase (Takara), and 25 μg/mL DNase-free RNase (Takara) were added into the three other dishes. These dishes were incubated at 37 °C in 5% CO_2 for 2 h. The cells were rinsed clean by PBS twice more before imaging. The fluorescent imaging pictures were obtained at an equal exposure time for the control, DNase, and RNase experiments.

Cytotoxicity Test. **CP** dye stock solutions were diluted by a fresh medium into three desired concentrations (1, 3, 5, 7, or 10 μM). The HeLa Cells were cultured in a 96-well plate for 12−24 h before the experiments. The cell medium was then replaced with different concentrations of **CP** dye medium solutions. These solutions were then incubated at 37 °C in 5% CO_2 for 24 h before the cell viability was measured by MTT assay. The cell medium solutions were replaced with 100 μL of a fresh medium, followed by the addition of 20 μL (5 mg/mL) of a MTT solution to each well. The cell plates were then incubated at 37 °C in 5% CO_2 for 4 h. The absorbance was measured at 570 nm, and that measured for an untreated cell population under the same experimental conditions was used as the reference point to establish 100% cell viability. The experiments have been duplicated.

Photostability Test. The HeLa cells were fixed in prechilled methanol at −20 °C for 1 min. Upon rinsing twice with PBS, the cells then were incubated in 1 mL of a PBS solution containing **CP1**, **CP3**, **CP6**, MTG, or RNASelect for 20 min. The cells were washed twice and then imaged by a confocal microscope (Nikon C1si). All of the dyes were continuously excited at 488 nm with equal laser power, and fluorescence was determined at the fluorescein isothiocyanate channel for RNASelect and at Cy5 for **CP** dyes through the no delay scan mode. The initial intensity referred to the first scan for each dye.

■ ASSOCIATED CONTENT

Ⓢ Supporting Information

X-ray crystallographic data in CIF format, characterization of the **CP** dyes, and supporting figures. This material is available free of charge via the Internet at http://pubs.acs.org.

■ AUTHOR INFORMATION

Corresponding Author

*E-mail: wangpf@mail.ipc.ac.cn.

Author Contributions

†These authors contributed equally to this work.

Notes

The authors declare no competing financial interest.

■ ACKNOWLEDGMENTS

This work was supported by the NNSF of China (Grants 21373250, 21173244, and F040801) and the Key Research Program of the Chinese Academy of Sciences (Grant KGZD-EW-T02).

■ REFERENCES

(1) Glancy, B.; Balaban, R. S. Role of Mitochondrial Ca^{2+} in the Regulation of Cellular Energetics. *Biochemistry* **2012**, *51*, 2959−2973.

(2) McBride, H. M.; Neuspiel, M.; Wasiak, S. Mitochondria: More Than Just a Powerhouse. *Curr. Biol.* **2006**, *16*, R551−R560.

(3) Abeliovich, A. Parkinson's Disease Mitochondrial Damage Control. *Nature* **2010**, *463*, 744−745.

(4) Appelqvist, H.; Waster, P.; Kagedal, K.; Ollinger, K. The Lysosome: From Waste Bag to Potential Therapeutic Target. *J. Mol. Cell Biol.* **2013**, *5*, 214−226.

(5) Luzio, J. P.; Pryor, P. R.; Bright, N. A. Lysosomes: Fusion and Function. *Nat. Rev. Mol. Cell Biol.* **2007**, *8*, 622−632.

(6) Boisvert, F. M.; van Koningsbruggen, S.; Navascues, J.; Lamond, A. I. The Multifunctional Nucleolus. *Nat. Rev. Mol. Cell Biol.* **2007**, *8*, 574−585.

(7) Boulon, S.; Westman, B. J.; Hutten, S.; Boisvert, F. M.; Lamond, A. I. The Nucleolus under Stress. *Mol. Cell* **2010**, *40*, 216−227.

(8) Leis, A.; Rockel, B.; Andrees, L.; Baumeister, W. Visualizing Cells at the Nanoscale. *Trends Biochem. Sci.* **2009**, *34*, 60−70.

(9) Bitgen, N.; Donmez Altuntas, H.; Hamurcu, Z.; Demirtas, H.; Ozturk, F. A Relation between the Agnors Motifs and T Lymphocyte Subgroups in Phytohemagglutinin-Stimulated Human T Lymphocytes. *Curr. Opin. Biotechnol.* **2011**, *22*, S115−S115.

(10) Gottwald, L.; Danilewicz, M.; Fendler, W.; Suzin, J.; Spych, M.; Piekarski, J.; Tylinski, W.; Chalubinska, J.; Topczewska-Tylinska, K.; Cialkowska-Rysz, A. The Agnors Count in Predicting Long-Term Survival in Serous Ovarian Cancer. *Arch. Med. Sci.* **2014**, *10*, 84−90.

(11) Savino, T. M.; Gebrane-Younes, J.; De Mey, J.; Sibarita, J. B.; Hernandez-Verdun, D. Nucleolar Assembly of the Rrna Processing Machinery in Living Cells. *J. Cell Biol.* **2001**, *153*, 1097−1110.

(12) Fujiwara, T.; Suzuki, S.; Kanno, M.; Sugiyama, H.; Takahashi, H.; Tanaka, J. Mapping a Nucleolar Targeting Sequence of an RNA Binding Nucleolar Protein, Nop25. *Exp. Cell Res.* **2006**, *312*, 1703−1712.

(13) Korgaonkar, C.; Hagen, J.; Tompkins, V.; Frazier, A. A.; Allamargot, C.; Quelle, F. W.; Quelle, D. E. Nucleophosmin (B23) Targets ARF to Nucleoli and Inhibits Its Function. *Mol. Cell. Biol.* **2005**, *25*, 1258−1271.

(14) Liu, B.; Shah, M.; Zhang, G.; Liu, Q.; Pang, Y. Biocompatible Flavone-Based Fluorogenic Probes for Quick Wash-Free Mitochondrial Imaging in Living Cells. *ACS Appl. Mater. Interfaces* **2014**, *6*, 21638−21644.

(15) Zhang, H.; Fan, J. L.; Wang, J. Y.; Zhang, S. Z.; Dou, B. R.; Peng, X. J. An Off-on Cox-2-Specific Fluorescent Probe: Targeting the Golgi Apparatus of Cancer Cells. *J. Am. Chem. Soc.* **2013**, *135*, 11663−11669.

(16) Masanta, G.; Lim, C. S.; Kim, H. J.; Han, J. H.; Kim, H. M.; Cho, B. R. A Mitochondrial-Targeted Two-Photon Probe for Zinc Ion. *J. Am. Chem. Soc.* **2011**, *133*, 5698−5700.

(17) Zhang, X.; Zhang, X.; Wang, S.; Liu, M.; Tao, L.; Wei, Y. Surfactant Modification of Aggregation-Induced Emission Material as Biocompatible Nanoparticles: Facile Preparation and Cell Imaging. *Nanoscale* **2013**, *5*, 147−150.

(18) Leung, C. W. T.; Hong, Y. N.; Chen, S. J.; Zhao, E. G.; Lam, J. W. Y.; Tang, B. Z. A Photostable AIE Luminogen for Specific Mitochondrial Imaging and Tracking. *J. Am. Chem. Soc.* **2013**, *135*, 62−65.

(19) Zhang, X. F.; Wang, C.; Han, Z.; Xiao, Y. A Photostable Near-Infrared Fluorescent Tracker with pH-Independent Specificity to Lysosomes for Long Time and Multicolor Imaging. *ACS Appl. Mater. Interfaces* **2014**, *6*, 21669−21676.

(20) Yang, Z.; He, Y.; Lee, J. H.; Chae, W.-S.; Ren, W. X.; Lee, J. H.; Kang, C.; Kim, J. S. A Nile Red/BODIPY-based Bimodal Probe Sensitive to Changes in the Micropolarity and Microviscosity of the Endoplasmic Reticulum. *Chem. Commun.* **2014**, *50*, 11672−11675.

(21) Buchwalow, I. B.; Böcker, W. *Immunohistochemistry: Basics and Methods*; Springer-Verlag GmbH & Co. K: Berlin, 2010.

(22) Fan, J. L.; Dong, H. J.; Hu, M. M.; Wang, J. Y.; Zhang, H.; Zhu, H.; Sun, W.; Peng, X. J. Fluorescence Imaging Lysosomal Changes During Cell Division and Apoptosis Observed Using Nile Blue Based Near-Infrared Emission. *Chem. Commun.* **2014**, *50*, 882−884.

(23) Egawa, T.; Hirabayashi, K.; Koide, Y.; Kobayashi, C.; Takahashi, N.; Mineno, T.; Terai, T.; Ueno, T.; Komatsu, T.; Ikegaya, Y.; Matsuki, N.; Nagano, T.; Hanaoka, K. Red Fluorescent Probe for Monitoring the Dynamics of Cytoplasmic Calcium Ions. *Angew. Chem., Int. Ed.* **2013**, *52*, 3874−3877.

DOI: 10.1021/acsami.5b01429
ACS Appl. Mater. Interfaces 2015, 7, 7421−7427

(24) Asanuma, D.; Takaoka, Y.; Namiki, S.; Takikawa, K.; Kamiya, M.; Nagano, T.; Urano, Y.; Hirose, K. Acidic-pH-Activatable Fluorescence Probes for Visualizing Exocytosis Dynamics. *Angew. Chem., Int. Ed.* **2014**, *53*, 6085−6089.
(25) Guo, Z. Q.; Park, S.; Yoon, J.; Shin, I. Recent Progress in the Development of near-Infrared Fluorescent Probes for Bioimaging Applications. *Chem. Soc. Rev.* **2014**, *43*, 16−29.
(26) Yuan, L.; Lin, W. Y.; Zheng, K. B.; He, L. W.; Huang, W. M. Far-red to Near Infrared Analyte-Responsive Fluorescent Probes Based on Organic Fluorophore Platforms for Fluorescence Imaging. *Chem. Soc. Rev.* **2013**, *42*, 622−661.
(27) Weissleder, R.; Ntziachristos, V. Shedding Light onto Live Molecular Targets. *Nat. Med.* **2003**, *9*, 123−128.
(28) Frangioni, J. V. In Vivo Near-Infrared Fluorescence Imaging. *Curr. Opin. Chem. Biol.* **2003**, *7*, 626−634.
(29) Lee, M. H.; Lee, S. W.; Kim, S. H.; Kang, C.; Kim, J. S. Nanomolar Hg(II) Detection Using Nile Blue Chemodosimeter in Biological Media. *Org. Lett.* **2009**, *11*, 2101−2104.
(30) Zhang, X.; Zhang, X.; Yang, B.; Zhang, Y.; Wei, Y. A New Class of Red Fluorescent Organic Nanoparticles: Noncovalent Fabrication and Cell Imaging Applications. *ACS Appl. Mater. Interfaces* **2014**, *6*, 3600−3606.
(31) Jiao, C. J.; Huang, K. W.; Guan, Z. P.; Xu, Q. H.; Wu, J. S. N-Annulated Perylene Fused Porphyrins with Enhanced Near-IR Absorption and Emission. *Org. Lett.* **2010**, *12*, 4046−4049.
(32) Jiao, C. J.; Huang, K. W.; Wu, J. S. Perylene-Fused Bodipy Dye with Near-IR Absorption/Emission and High Photostability. *Org. Lett.* **2011**, *13*, 632−635.
(33) Chen, J. H.; Liu, W. M.; Ma, J. J.; Xu, H. T.; Wu, J. S.; Tang, X. L.; Fan, Z. Y.; Wang, P. F. Synthesis and Properties of Fluorescence Dyes: Tetracyclic Pyrazolo[3,4-*b*]Pyridine-Based Coumarin Chromophores with Intramolecular Charge Transfer Character. *J. Org. Chem.* **2012**, *77*, 3475−3482.
(34) Yuan, L.; Lin, W. Y.; Yang, Y. T.; Chen, H. A Unique Class of near-Infrared Functional Fluorescent Dyes with Carboxylic-Acid-Modulated Fluorescence On/Off Switching: Rational Design, Synthesis, Optical Properties, Theoretical Calculations, and Applications for Fluorescence Imaging in Living Animals. *J. Am. Chem. Soc.* **2012**, *134*, 1200−1211.
(35) Xiong, X. Q.; Song, F. L.; Chen, G. W.; Sun, W.; Wang, J. Y.; Gao, P.; Zhang, Y. K.; Qiao, B.; Li, W. F.; Sun, S. G.; Fan, J. L.; Peng, X. J. Construction of Long-Wavelength Fluorescein Analogues and Their Application as Fluorescent Probes. *Chem.—Eur. J.* **2013**, *19*, 6538−6345.
(36) Bochkov, A. Y.; Akchurin, I. O.; Dyachenko, O. A.; Traven, V. F. NIR-Fluorescent Coumarin-Fused Bodipy Dyes with Large Stokes Shifts. *Chem. Commun.* **2013**, *49*, 11653−11655.
(37) Chen, J. H.; Liu, W. M.; Zhou, B. J.; Niu, G. L.; Zhang, H. Y.; Wu, J. S.; Wang, Y.; Ju, W. G.; Wang, P. F. Coumarin- and Rhodamine-Fused Deep Red Fluorescent Dyes: Synthesis, Photophysical Properties, and Bioimaging in Vitro. *J. Org. Chem.* **2013**, *78*, 6121−6130.
(38) Zhou, B. J.; Liu, W. M.; Zhang, H. Y.; Wu, J. S.; Liu, S.; Xu, H. T.; Wang, P. F. Imaging of Nucleolar RNA in Living Cells using a Highly Photostable Deep-red Fluorescent Probe. *Biosens. Bioelectron.* **2015**, *68*, 189−196.
(39) Haucke, G.; Czerney, P.; Igney, C.; Hartmann, H. Absorption-Spectra and Fluorescence Behavior of Benzopyrylium Compounds. *Ber. Bunsen-Ges. Phys. Chem.* **1989**, *93*, 805−815.
(40) Knight, T. E.; Goldstein, A. P.; Brennaman, M. K.; Cardolaccia, T.; Pandya, A.; DeSimone, J. M.; Meyer, T. J. Influence of the Fluid-to-Film Transition on Photophysical Properties of Mlct Excited States in a Polymerizable Dimethacrylate Fluid. *J. Phys. Chem. B* **2011**, *115*, 64−70.
(41) Sommer, J. R.; Shelton, A. H.; Parthasarathy, A.; Ghiviriga, I.; Reynolds, J. R.; Schanze, K. S. Photophysical Properties of Near-Infrared Phosphorescent π-Extended Platinum Porphyrins. *Chem. Mater.* **2011**, *23*, 5296−5304.
(42) Ueno, Y.; Jose, J.; Loudet, A.; Perez-Bolivar, C.; Anzenbacher, P.; Burgess, K. Encapsulated Energy-Transfer Cassettes with Extremely Well Resolved Fluorescent Outputs. *J. Am. Chem. Soc.* **2011**, *133*, 51−55.
(43) Song, G. F.; Sun, Y. M.; Liu, Y.; Wang, X. K.; Chen, M. L.; Miao, F.; Zhang, W. J.; Yu, X. Q.; Jin, J. L. Low Molecular Weight Fluorescent Probes with Good Photostability for Imaging RNA-Rich Nucleolus and RNA in Cytoplasm in Living Cells. *Biomaterials* **2014**, *35*, 2103−2112.
(44) Magde, D.; Brannon, J. H.; Cremers, T. L.; Olmsted, J. Absolute Luminescence Yield of Cresyl Violet—Standard for the Red. *J. Phys. Chem.* **1979**, *83*, 696−699.

DOI: 10.1021/acsami.5b01429
ACS Appl. Mater. Interfaces 2015, 7, 7421−7427